

Provided for non-commercial research and education use.  
Not for reproduction, distribution or commercial use.



This article appeared in a journal published by Elsevier. The attached copy is furnished to the author for internal non-commercial research and education use, including for instruction at the authors institution and sharing with colleagues.

Other uses, including reproduction and distribution, or selling or licensing copies, or posting to personal, institutional or third party websites are prohibited.

In most cases authors are permitted to post their version of the article (e.g. in Word or Tex form) to their personal website or institutional repository. Authors requiring further information regarding Elsevier's archiving and manuscript policies are encouraged to visit:

<http://www.elsevier.com/authorsrights>



Contents lists available at ScienceDirect

# Journal of Wind Engineering and Industrial Aerodynamics

journal homepage: [www.elsevier.com/locate/jweia](http://www.elsevier.com/locate/jweia)

## Combined effect of jet impingement and density perturbation forcing on the evolution of laboratory-simulated microbursts



G. Demarco<sup>b,\*</sup>, N. Barrere<sup>a</sup>, G. Sarasúa<sup>a</sup>, A.C. Martí<sup>a</sup>, O.C. Acevedo<sup>b</sup>, E. Nascimento<sup>b</sup>,  
C. Cabeza<sup>a,\*\*</sup>

<sup>a</sup> Instituto de Física, Facultad de Ciencias, Universidad de la República, Uruguay

<sup>b</sup> Universidade Federal de Santa Maria, Departamento de Física, Santa Maria, RS, Brazil

### ARTICLE INFO

#### Article history:

Received 28 November 2012

Received in revised form

7 August 2013

Accepted 10 August 2013

Available online 31 October 2013

#### Keywords:

Microburst

Turbulence

Experimental simulation

### ABSTRACT

A laboratory simulation was assessed for its capacity to reproduce the actual conditions found in a microburst. In our experimental set-up, the flow was driven by combined impinging jet and density perturbations forcing with the aim of determining their relative influence on the overall microburst behavior and, in particular, the initiation and structural evolution of the resulting vortex. These results were compared with those reported in the previous simulation works. Such comparisons showed that the laboratory model may satisfactorily reproduce relevant aspects of a microburst. An expression for the characteristic microburst propagation velocity was derived, accounting for the combined effects of forced velocity and flotation forces generated by the density difference, whose predictions are in good agreement with experimental data. The vortex structure is largely affected by the forcing type. The succession of vortex is best defined when a large density perturbation is combined with a weak jet impingement. The opposite configuration causes a main vortex to be succeeded by a wake where vortex structures are not clearly defined. Such behavior is caused by the fact that larger density perturbations inhibit the mean and turbulent velocities, favouring a well defined vortices structure, associated with weaker momentum diffusion.

© 2013 Elsevier Ltd. All rights reserved.

### 1. Introduction

Severe convectively generated winds called downbursts have received much attention in the fields of meteorology, civil engineering and aviation (Fujita, 1985, 1990; Wakimoto, 2001). The underlying phenomenon may be explained in terms of a very intense downdraft originated from a thunderstorm (or thunderstorm system) that, after impinging on the ground surface, leads to strongly divergent winds at and just above the ground level. Such winds can reach more than  $30 \text{ ms}^{-1}$  and spread laterally over an area of up to several tens of kilometers in radius. Occurring typically over a small spatial scale, these winds are associated with high shear forces, being capable of producing significant damage to buildings and representing a serious threat to aircrafts, especially during landing and takeoff maneuvers (Fujita, 1985, 1990). A microburst is usually defined as a downburst with horizontal extent of less than 4 km, with a lifetime ranging from 2 to 5 min (Proctor, 1988; Wakimoto, 2001). When the radius of the divergent outflow is greater than 4 km, and lasts for more than 5 min, the phenomenon is sometimes referred to as a macroburst.

A considerable number of fatal aviation accidents have been attributed to the occurrence of microbursts (Fujita, 1990).

One remarkable characteristic of microbursts is the formation of a ring-shaped vortex that expands radially following the impingement of the downdraft on the ground surface and the formation of the outflow (Fujita, 1990). The evolution of such vortex is a crucial aspect to better understand important dynamic features of microbursts.

Despite a few successful field studies addressing microbursts and similar phenomena (e.g., Fujita, 1985; Hjelmfelt, 1988, and Weisman, 1993), and the highly localized and hard-to-predict nature of the phenomenon make it difficult for adequate data collection. Therefore, both numerical (Proctor, 1988; Kim and Hangan, 2007; Vermeire et al., 2011; Anabor et al., 2011) and laboratory simulations (Landreth and Adrian, 1990; Lundgren et al., 1992; Mason et al., 2005) have been used widely for the study of microbursts basic dynamics. Whether numerical or experimental, simulations are based on two main approaches with regard to the driving mechanism that initiates a gravity current used as a proxy for a microburst. The impinging jet approach (Landreth and Adrian, 1990; Mason et al., 2005; Kim and Hangan, 2007) is based on the prescription of a vertical current of fluid impinging on a flat ground surface. Alternatively, the cooling source approach (Proctor, 1988; Lundgren et al., 1992; Vermeire et al., 2011) is based on the vertical collapse of a denser fluid from an initial position at a certain height which is allowed to spread laterally within a lighter fluid after reaching a ground surface. Such density

\* Corresponding author.

\*\* Principal corresponding author. Tel.: +598 25258624; fax: +598 25250580.

E-mail addresses: [giulianofisico@gmail.com](mailto:giulianofisico@gmail.com) (G. Demarco),  
[cecilia@fisica.edu.uy](mailto:cecilia@fisica.edu.uy) (C. Cabeza).

difference – in analogy to the density difference generated by the evaporative cooling of raindrops in a thunderstorm – may be simulated by the addition of salts or the cooling an aqueous fluid. Vermeire et al. (2011) compared numerical simulations based on the impinging jet approach with others based on the cooling source approach and concluded that the former did not account for certain distinct characteristics of actual microburst occurrences. Nonetheless, in view of the number of studies based on each of the two types of initiation process of the microburst-like gravity current, a better understanding of how comparisons may be conducted between the two general procedures are desirable.

Previous microburst simulation studies have consistently reported the formation of a primary horizontally oriented vortex at the leading edge of the phenomenon (e.g., Proctor, 1988; Anabor et al., 2011), which is also mentioned in observational studies of microbursts (Wakimoto, 2001). Regardless of the mechanism used for the initiation of the gravity current in the simulations, results differ in the structure of such primary vortex (Mason et al., 2005), referred to in the literature as a primary eddy. Pulsating vorticity perturbations, sometimes apparent from direct observation of microbursts, suggest the possibility of secondary vortex (Hjelmfelt, 1987, 1988). Using either a cooling source (Proctor, 1989) or an impinging jet numerical simulation (Landreth and Adrian, 1990), an intermediate vortex has been reported to form behind the propagation the primary eddy. The formation of an intermediate vortex was observed experimentally by Mason et al. (2005), while Kim and Hangan (2007) reported the occurrence of a well-defined intermediate vortex using impinging jet numerical simulation. A secondary maximum of strong winds was also described in the large eddy simulations by Anabor et al. (2011).

This paper describes the results from laboratory simulations of microburst like gravity currents that combine the impinging jet and cooling source (mimicked by the prescription of a positive density perturbation) approaches. The goal is to further analyze the combined effects of such two driving mechanisms on the behavior of the microburst like flow and on the formation and propagation of primary and secondary vortices. The discussion is aimed at providing a more detailed physical insight on previous studies that are based on each of the existing approaches separately. This study also highlights the conditions affecting (either positively or negatively) the development and maintenance of secondary vortex and wind maxima trailing the leading front of the phenomenon.

## 2. Experimental setup

In this work, density currents used as dynamical models for microbursts were simulated in laboratory by providing a continuous vertical (top-down) injection of a higher-density fluid into a lower-density fluid environment. Using water as such fluid, prescribed density anomalies were controlled by the addition of salt (NaCl) at different concentrations to the injected fluid. Fig. 1 shows the schematic experimental setup. The flow rate was measured using a digital flow sensor (not shown in the figure) with a full-scale relative accuracy of 1%. Table 1 shows the working flow rates and density differences. The notation used in Table 1 is as follows: the first three digits indicate the flow rate used and the last two the density difference between the jet and the environment. An overflow tank system was used to maintain a constant flow rate during all the experiment. Given that the experience lasts about 15–20 s, for the flow rates used, it can be assumed that the height  $H=10$  cm is constant within a relative error of 0.5–1%. The Reynolds number, calculated based on the inflow velocity into the environment of study, amounted to  $Re_1=10^3$  and  $Re_2=1.5 \times 10^3$  in experimental conditions using 300 ml/min and 500 ml/min, respectively.

A standard digital particle image velocimetry (DPIV) technique was implemented to obtain the velocity fields (Westerweel, 1997,

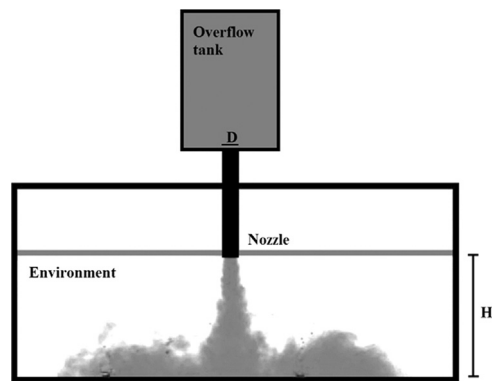


Fig. 1. Schematic representations of experimental setup.

**Table 1**  
Experimental parameters and respective notations.

Experiment	Flow rate (ml/min)	$\Delta\rho$ (%)
30005	300	0.5
50005	500	0.5
30010	300	1.0
50010	500	1.0

2000). This technique allows to get accurate quantitative values of the velocity profiles based on the cross-correlation of two consecutive images. In this work, the fluid was seeded with neutral buoyant polyamide particles 50  $\mu\text{m}$  in diameter. For the present values of the velocities, the particles, in the Stokes regime, do not disturb the flow and follow accurately the streamlines. A Nd:YAG laser (500 mW) and a cylindrical lens was used to illuminate a plane (2 mm thick) containing the microburst axis. The light scattered by the particles is then captured on a series of images using a CMOS camera set at 50 frames per second (fps).

Velocity fields were derived by the use of standard cross-correlation algorithms between two consecutive acquired images (Adrian, 1991). Each image is divided up into regions called interrogation windows of  $64 \times 64$  pixels and 50% overlap and they are correlated to determine statically the average particle displacement over the interrogation area. This procedure is repeated for all interrogation areas and a displacement vector map is created for the image space. Dividing the displacement vector map by the time lag between two consecutive images produces the two velocity components parallel to the illuminated plane.

The relevant experimental parameters are the height of the inlet nozzle ( $H$ ), the nozzle diameter ( $d=6.8$  mm), the density difference ( $\Delta\rho$ ), the kinematics viscosity ( $\nu$ ), and the heavy fluid inflow velocity ( $U$ ), the latter relating to the flow rate according to the equation  $Q = \pi U d^2 / 4$ . These parameters were used for the generation of dimensionless numbers  $Re = Ud/\nu$ , the Reynolds number,  $F = U/\sqrt{g'H}$ , the Froude number, where  $g' = g\Delta\rho/\rho$  is the reduced gravity and the aspect ratio  $\zeta = d/h$ . As  $\zeta$  has been kept at a constant value through all runs,  $Re$  and  $F$  alone may be used to characterize the experimental hydrodynamic conditions.

According to our experimental results, a change in  $F$  was associated with a change in the characteristic time of system evolution, whereas a change in  $Re$  was associated with a slight change in the flow pattern. These findings are consistent with the previous studies reporting this dependence at low Reynolds values (Lundgren et al., 1992). Nonetheless, such changes in flow pattern are only small and, in actual practice, do not result in significant changes in the overall microburst structure with respect to the

model proposed by Proctor (1988). It shows that although variations of  $Re$  produces changes in the flow, the overall structure is not modified in an important way. This is also in agreement with the results obtained by Kim and Hangan (2007) concerning the flow profile. For determining the Froude number, the diameter of the jet  $D$  has been chosen as characteristic length scale. In the case of Proctors simulation, the characteristic scales can be estimated as  $U \approx 20$  m/s,  $D \approx 1$  km, while the reduced gravity can be found from the state equation of the ideal gas ( $\Delta\rho/\rho = \Delta T/T$ ). Further assuming that  $\Delta T \approx 10$  °C,  $T \approx 280$  K, it leads to  $F \approx 1$  in Proctors data. In the present experiment,  $U \approx 1.18$  m/s, and it leads to  $F \approx 6$ . This means that, although the Reynolds numbers are very different, the Froude numbers are of the same order in our experiment and in Proctors simulation. This explains why our experiments exhibit similar structure to those obtained in Proctor's study.

The system was able to determine the velocity components in two directions, one horizontal ( $x$ ), which will be sometimes also referred as radial and the vertical height ( $y$ ). For each simulation, fields of the radial and vertical velocity components ( $v_r$  and  $v_y$ , respectively) were obtained. Each field is typically composed of 108 points in  $x$ , 49 in  $y$  and 999 temporal frames. The convention used for the signs of the velocity is as follows:  $v_r$  is positive outward from the axis of the microburst and  $v_y$  is positive upwards.

Most analyses used the instantaneous values or averages over one or two dimensions. The frontal position of the main vortex as it propagated was objectively determined through the identification of the first position in which the magnitude of the velocity vector exceeded 0.001 m/s for each time frame, in all experiments. Likewise, the vortex center has been assumed as the first position upstream of the vortex front where the velocity vector decreases in magnitude.

### 3. Vortex formation and propagation

These experimental results depict the instability generated by the shearing effect of a flux of fluid impinging onto a surface. As a result of the horizontal shear on the edge of vertical jet, vorticity field was generated characterizing a primary vortex, which then spread over the ground surface, as seen in Fig. 2. Similar results were obtained for the other experimental conditions tested. The vortex increased in size as it traveled radially at an approximately constant velocity.

Fig. 3 shows the effect of  $Q$ , the downward flow rate, and that of  $\Delta\rho$ , the density difference between the heavy, downward fluid and the lighter, environmental fluid. Whereas all evolution curves are similar in shape, the vortex was found to propagate at different velocities depending on the relevant parameters. The highest

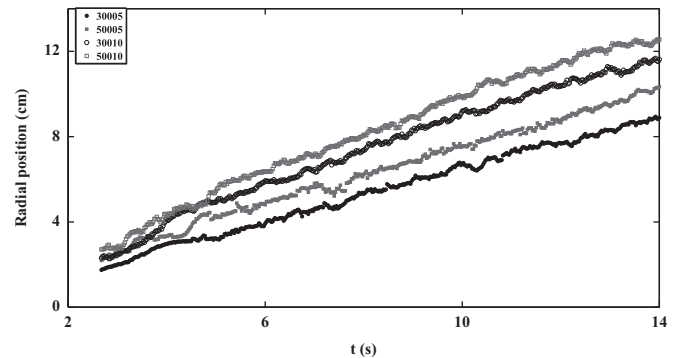


Fig. 3. Vortex position as a function of time for different experimental conditions (see Table 1).

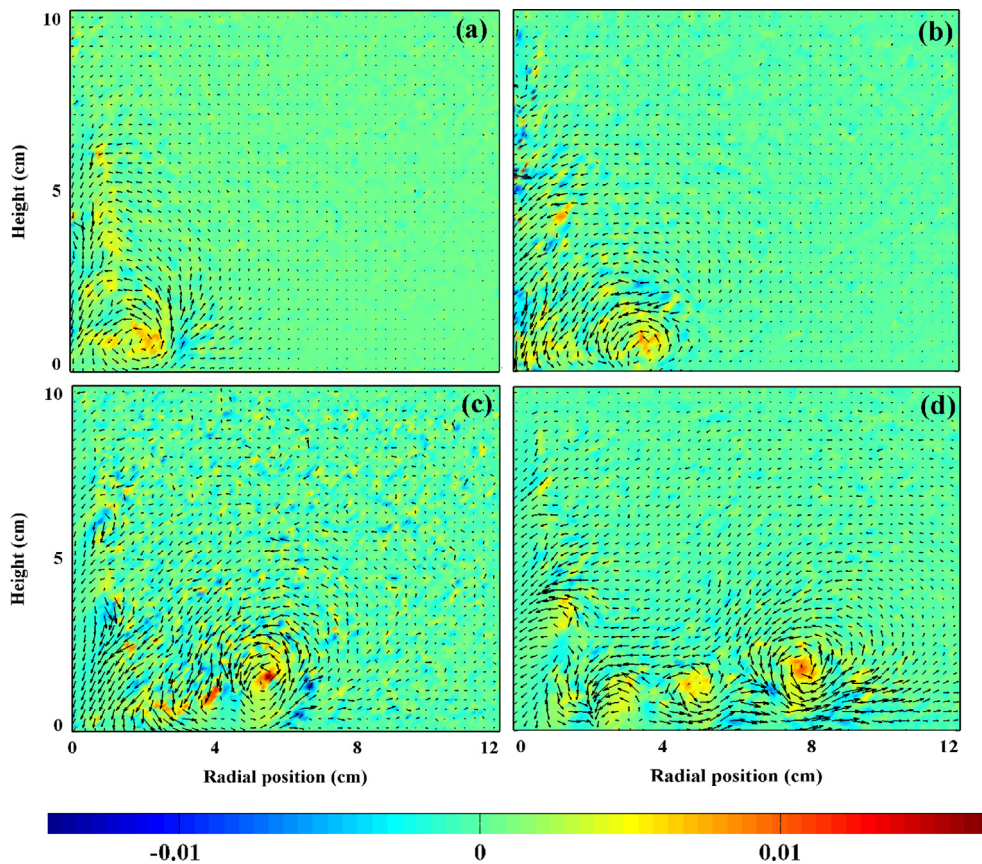


Fig. 2. Snapshots of the velocity field (arrows) and the corresponding vorticity field (color code) for experiment 30005. (a)  $t=3$  s; (b)  $t=6$  s; (c)  $t=9$  s; (d)  $t=13.9$  s. The time when the fluid impinges first the ground surface was taken as reference ( $t=0$  s). (For interpretation of the references to color in this figure caption, the reader is referred to the web version of this article.)

propagation velocity was noted when the combined effects of flow rate and density difference were most intense, i.e., for experiment 50010. Likewise, the lowest  $Q$  and  $\Delta\rho$  values used in the study (experiment 30005) were associated with the lowest vortex propagation velocity. Interestingly, experiments 30010 and 50005 had similar propagation velocities despite the difference in both forcing between them. Because the curves of evolution of the vortex position as a function of time were similar for all the experiments studied, they were re-scaled based on the characteristic time, whose value differed for each experimental run.

Considering a downward current of fluid driven spontaneously by gravity (cooling source), a scaling law may be derived wherein the perturbation is expressed in terms of the density value,  $\rho$ , at a point located in a resting environment where the density is  $\rho_0$  (Lundgren et al., 1992). The characteristic time of the density perturbation may be defined as a function of  $R_0$ , a characteristic length, and  $\Delta\rho$ , a density difference, according to the following expression:

$$T_{\Delta\rho} = \sqrt{\left(\frac{R_0\rho}{g\Delta\rho}\right)} \quad (1)$$

In our experimental set-up, the jet was generated by  $\Delta\rho$ , the density difference, and  $U$ , the forced velocity of the jet, so that the characteristic time may be described by a more complex equation that accounts for both contributions. Neglecting the effect of viscosity, the

characteristic velocity  $V_0$  of the jet depends on  $H$ , the reduced gravity  $g'$  and the fluid velocity  $U$ . Two independent dimensionless numbers may be thus defined:  $V_0/U$  and  $V_0/V_\rho$ , wherein

$$V_\rho = \sqrt{Hg'} \quad (2)$$

According to the Vaschy–Buckingham theorem, it may be stated that

$$V_0 = f(U, V_\rho) \quad (3)$$

wherein  $f$  is a certain function. Based on a linear approximation of the function over a certain region, the  $V_0$  equation may be written as

$$V_0 = k_1U + K_2V_\rho + c \quad (4)$$

wherein  $c$  is a constant. Considering that  $U$  is the dominant term, and that  $V_\rho$  is a corrective value,  $c$  is assumed to be negligible (if  $V_\rho = 0$ , then  $V_0$  equals  $U$ , so that  $c=0$ ). Therefore, an equation of the following type was considered:

$$V_0 = U + KV_\rho \quad (5)$$

wherein  $K$  is a dimensionless constant. The characteristic time, such that  $T_0 = R_0/V_0$ , may be derived from the above equation. The vortex evolution was compared by means of  $t/T_0$ , a dimensionless time, using  $K=3.1$  consistently in all cases, and the resulting curves were found to overlap reasonably as shown in Fig. 4.

#### 4. Velocity profiles

Our experimental results were compared with those reported by Proctor (1988) and those reported in more recent works (Holmes and Oliver, 2000; Mason et al., 2005; Kim and Hangan, 2007; Anabor et al., 2011). The main focus is in the comparison to the results from Proctor (1988), because this is a classical, recognized work, whose simulations were performed in very realistic conditions, reproducing the actual conditions of atmosphere. Initially, an analysis was made of the radial velocity at a fixed height, see Proctor (1988, Fig. 5). To enable a comparison of qualitative results, the appropriate shift in the time variable was made in order to account for the points of time used as reference, which, in the case of Proctor's model, was defined as the start of the simulation, and, in this work, was set at the time of impingement, i.e.,  $t_g=6$  min.

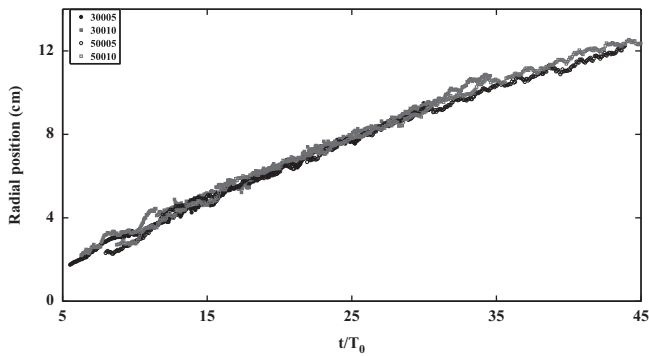


Fig. 4. Propagation velocity of the front for different configurations. Time scale is the same for the settings used.

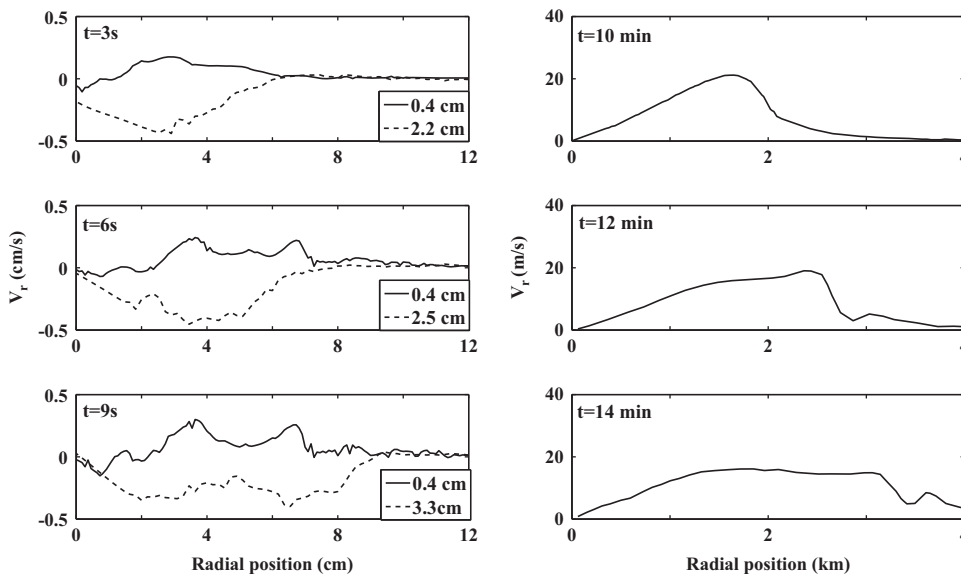


Fig. 5. Radial velocity profiles as a function of the distance to the microburst axis at different times indicated in each panel. Left column corresponds to experiment 30005 and right column is extracted from Fig. 5c–e (Proctor, 1988). In the left column dashed (full) lines correspond to a location above (below) the vortex core represented in Fig. 2. In the experiments, the levels of the vortex core are located at 0.6 cm, 0.8 cm and 1.5 at, respectively  $t=3$  s,  $t=6$  s, and  $t=9$  s.

Fig. 5 shows radial velocity profiles at different heights from the ground. The sign convention used is positive for outward propagation. Fig. 5a, constructed at  $t=3$  s, shows a single maximum positive clearly visible at  $y=0.4$  cm, bottom of vortex, and presents a maximum negative at  $y=2.2$  cm, corresponding to top of the vortex. The above is consistent with that suggested by Fig. 5 in Proctors work. It is to be noted that the curve changes in shape and begins to show a minimum in addition to the above maximum with increasing height. This minimum cannot be observed in Proctors work due to the low height value used for the analysis with respect to the vortex size (considering a height not smaller than 60 m would be adequate for a vortex size of the order of 600 m).

At  $t=6$  s and  $t=9$  s, two maxima positive were noted for the height  $y=0.4$  cm. Consistently with these results, the minimum and the two maxima are also found in Proctors (Fig. 5d and e). A similar situation corresponding to maximum negative the above may be noted. The above suggests that the minima observed in Proctors curves at  $t'$  values greater than 6 min would have been noted at an earlier time if higher height values had been used for the analysis. In light of all the above, Proctors curves were found consistent with the experimental results obtained for the lowest height value used in this study.

Conclusions regarding vortex height and evolution may be drawn from the observation of a sign change in radial velocity (Fig. 6). At  $t=3$  s, the vortex had already reached the position  $r=2.0$  cm from the axis of the downflow column (full-line), but had clearly not yet reached the farther positions shown by the dotted-line ( $r=4.1$  cm)

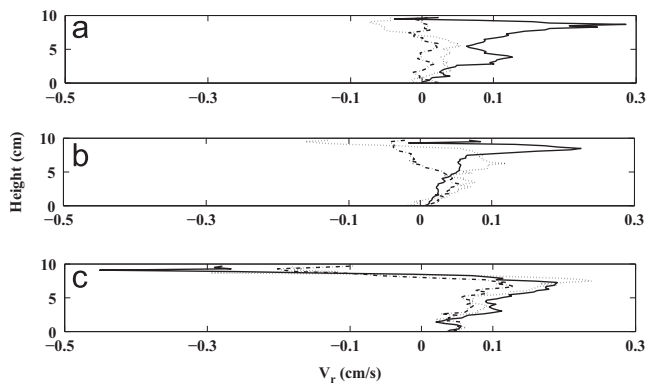


Fig. 6. Radial velocity  $v_r$  profiles as a function of height, at radial positions where  $v_r$  is maximum, in experiment 30005: (a)  $t=3$  s; (b)  $t=6$  s; (c)  $t=9$  s. Full-line corresponding to  $r=2$  cm, dotted-line  $r=4.1$  cm and dashed-line  $r=6.9$  cm.

and the dashed-line ( $r=6.9$  cm). With the passage of time, (Fig. 6b and c) the vortex reached all the observation points.

Fig. 7 shows vertical velocity profiles as a function of time, keeping the height selected for the analysis at a fixed value. Our qualitative results were also found consistent with the numerical results reported by Proctor (1988). The evolution pattern noted from our experimental results at  $t$  values greater than 6 s (Fig. 7a–c) were found consistent with Proctor (1988, Fig. 5), where, at  $t'=2$  min, the vertical velocity  $v_y$  shows a minimum at  $r=0$  cm and a slight maximum, whereas at  $t'$  greater than 4 min, two maxima are noted at a close distance.

Vermeire et al. (2011) compared the velocity profiles in the position of maximum radial velocity for simulations of jet impingement and cooling source separately. The analysis showed important differences in the profiles between the two types of simulation. Vermeire et al. (2011) concluded that the impinging jet simulations may not be realistic enough. We perform a similar analysis at the vortex front position in order to investigate how the two effects combine (Fig. 8, left panel). The two experiments with

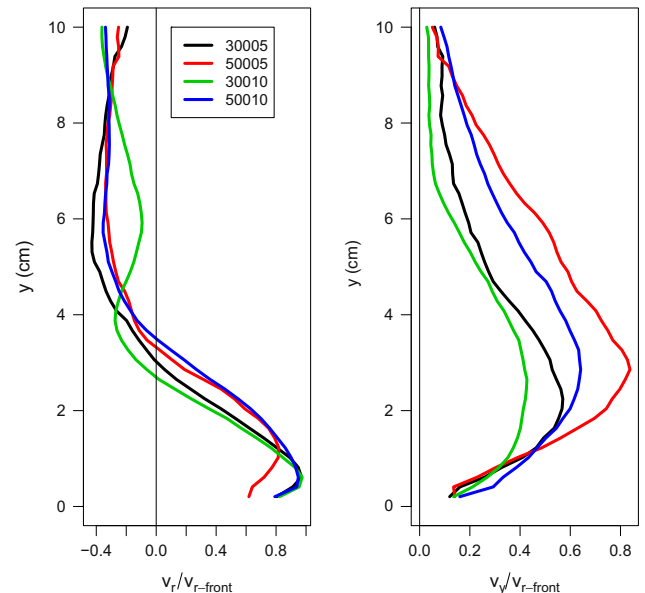


Fig. 8. Vertical profiles of radial and vertical velocities at the position where the maximum radial velocity was verified for the different experiments. Values have been normalized by the radial velocity at the vortex frontal position.

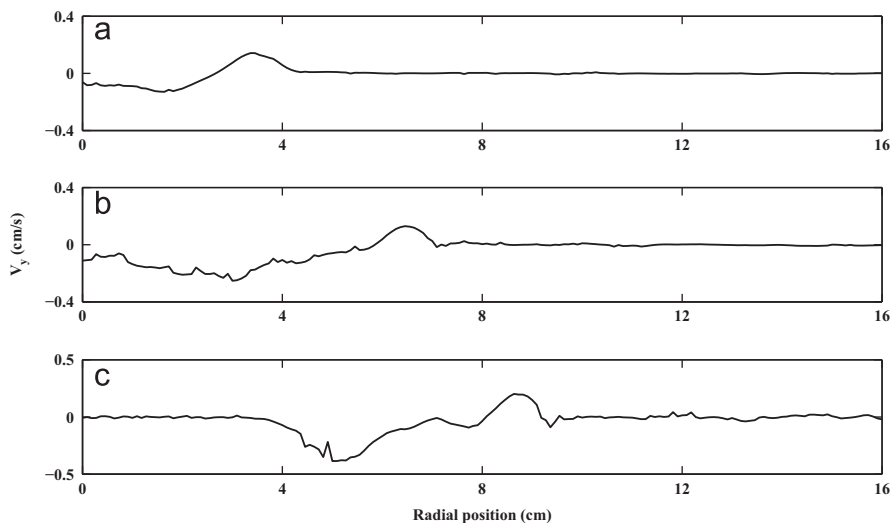


Fig. 7. Vertical velocity profiles as a function of distance to the microburst axis, for down level to the vortex core (experiment 30005). (a)  $t=3$  s; (b)  $t=6$  s; (c)  $t=9$  s.

more intense jets (50005 and 50010 experiments) show higher radial velocity over a deeper layer, similarly to what occurs in the jet impingement simulations by Vermeire et al. (2011). At the same time, experiment 30010, for which the relative importance of the density perturbation is largest, is the one with closest agreement to Vermeire et al. simulation with cooling source (i.e., is the one with sharpest vertical decay of radial velocity). Concerning the vertical velocity profiles, the present results (Fig. 8, right panel) show that the stronger impinging jet causes the highest and the most intense peak. Both findings are in agreement with the results from Vermeire et al. (2011). Greater density perturbations always reduce the vertical velocity in relation to those that occur in simulations with low density perturbation.

### 5. Vortex structure

The propagation velocity of the primary vortex is not the only characteristic affected by the jet velocity and the density perturbation. Another property greatly affected is the vortex structure, which here refers to the number of vortex observed simultaneously, and their spatial coherence in each moment. This fact can be appreciated in Fig. 9, where all panels refer to the same time frame. In the experiment 30005 the primary vortex reaches 3 cm in height and is followed by secondary vortices which appear to merge with each other. For the experiment 50005, the most intense and well-defined vortex reaches 4 cm in height and there are no well-defined intermediate vortices.

When the density perturbation increases to  $\Delta\rho/\rho=1\%$ , the vertical extension of the primary vortex decreases to 2 cm (Fig. 9) and it is followed by the appearance of better defined secondary vortices. In the experiment 30010, it is possible to identify precisely

three secondary vortices, while in the experiment 50010, two of these appear to merge with each other. A consequence of the succession of vortices is the emergence of vorticity dipoles.

The vortex organization and distribution during the experiments can be accurately depicted when comparing the vertically averaged vorticity, given by  $\eta = (\partial v_y/\partial x) - (\partial v_r/\partial y)$ , as a function of the radial position and time (Fig. 10). In all panels, the vortices are identified by regions of maximum vorticity. Highest vorticity values are found in the experiment 50005. At the same time the experiment 50005 displays the most disorganized pattern of secondary vortices. The wide primary vortex mingles with the secondary ones on its wake. In contrast, experiment 30010 is the one that shows the weakest primary vortex and, at the same time, the best-defined succession of secondary vortices.

Interestingly, despite showing such contrasting vortex structures, experiments 50005 and 30010 exhibit somewhat similar vortex propagation velocities in Fig. 3. In between these two extremes, in experiments 30005 and 50010, well-defined secondary vortices occur only for limited time periods. Thus, while the combination of the impinging jet and density perturbation forcings produced similar vortex propagation velocity it also produced opposite effects in terms of the primary vortex intensity and coherence of the secondary vortices.

In order to investigate such findings in more detail, we analyze the average magnitude of the velocity vector over time depicted in Fig. 11. The experiment 50005 showed the highest instantaneous velocity, while the experiment 30010 displayed lowest instantaneous velocities. Turbulent velocities are highly correlated with the mean velocity magnitude. Fig. 12 presents the profiles of the turbulent velocity scale  $V_T$ , defined as

$$V_T = \sqrt{\frac{1}{2}(\sigma_{v_r}^2 + \sigma_{v_y}^2)}$$

where  $\sigma_{v_r}$  and  $\sigma_{v_y}$  are, respectively, the temporal standard deviations of the fluctuations of velocity components  $v_r$  and  $v_y$ , calculated for groups of 50 time frames. Such profiles confirm that experiment 50005 is the most turbulent, while 30010 is the least turbulent of all. Thus, the results indicate that higher values of velocity and turbulence are associated with less organized vortices, suggesting that in these cases there is also more turbulent diffusion of momentum. This greater horizontal diffusion may, therefore, be responsible for the lack of organization of the intermediate vortices in experiment 50005, with the opposite causing the greater organization in the experiment 30010.

When comparing the profiles and the velocity magnitudes both at leading edge and inside the primary vortex, as shown in Fig. 13, we noted that the perturbation density has a direct role in reducing average and turbulent velocity. At the front of the vortex, the velocity magnitude is modulated mainly by the velocity of the impinging jet. That is, the strongest velocity magnitudes occur in simulations where the jet flux is 500 ml/min, as can be seen in Fig. 13, left panel. The density perturbation, in turn, plays only a secondary role on influencing the velocity magnitude in that position. When the same analysis is conducted in the center of the vortex, depicted in Fig. 13, right panel, we find that the density perturbation becomes the most important factor modulating the velocity magnitude, with highest values occurring when the perturbation density is the least. Moreover, a significant increase in velocity magnitude also becomes apparent at the center of the vortex as compared to its leading edge.

### 6. Conclusions

Our results show that the experimental set-up used in this study was capable of quantitatively reproducing a microburst. The conclusion is supported by comparison of these results with those

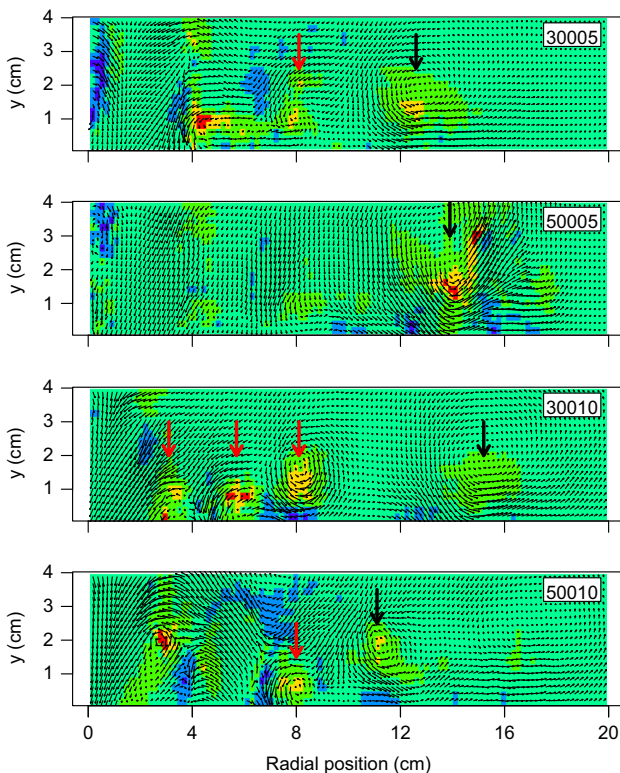


Fig. 9. Velocity vectors (arrows) and horizontal vorticity (colors) for the different experiments, corresponding to  $t=18$  s of experiment. Primary vortices are identified by black arrows, and secondary vortices by red arrows. (For interpretation of the references to color in this figure caption, the reader is referred to the web version of this article.)

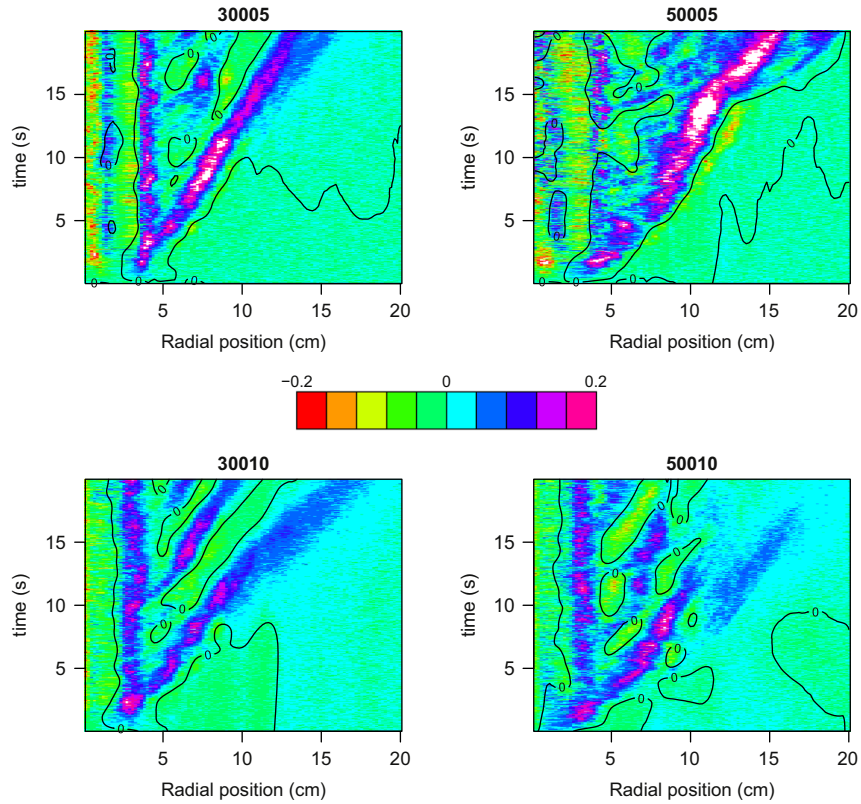


Fig. 10. Vertically averaged horizontal vorticity as a function of radial position and time, for each experiment, as indicated at the top of each panel.

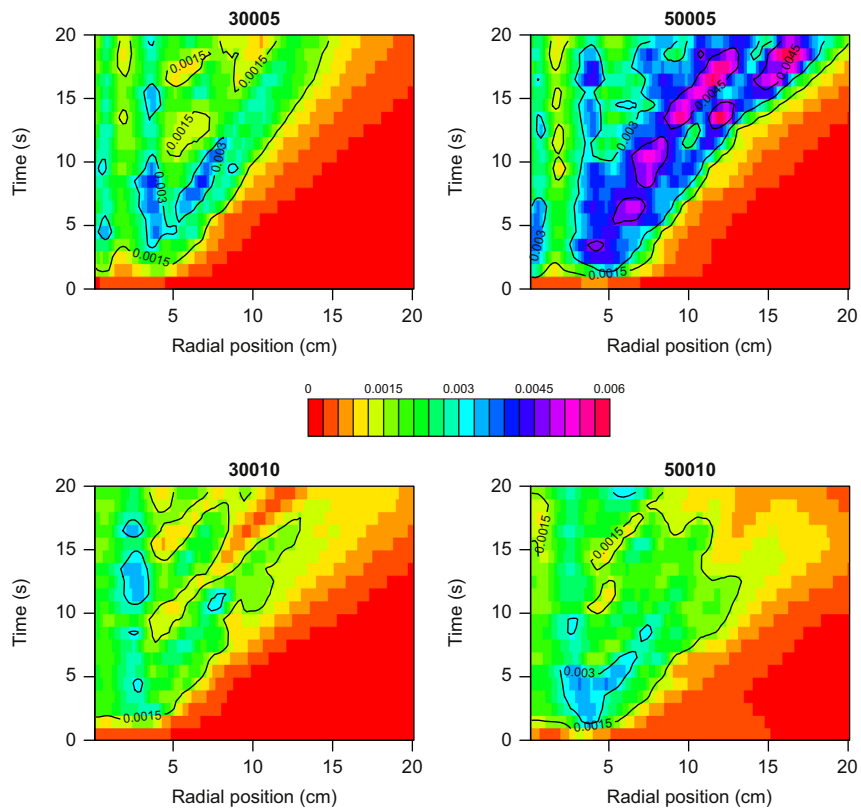


Fig. 11. Mean turbulent velocity scale as a function of radial position and time, for each experiment, as indicated at the top of the panels. Temporal averages were calculated for groups of 50 frames.

reported by Proctor for numerical simulations in conditions reproducing actual atmospheric environments. A solid degree of consistency was found between the data from both works, finding

maximum velocities to be associated with the presence of the vortex. Our analysis considered the dependence of overall microburst evolution on both jet velocity variations (i.e.,  $Re$ ) and density

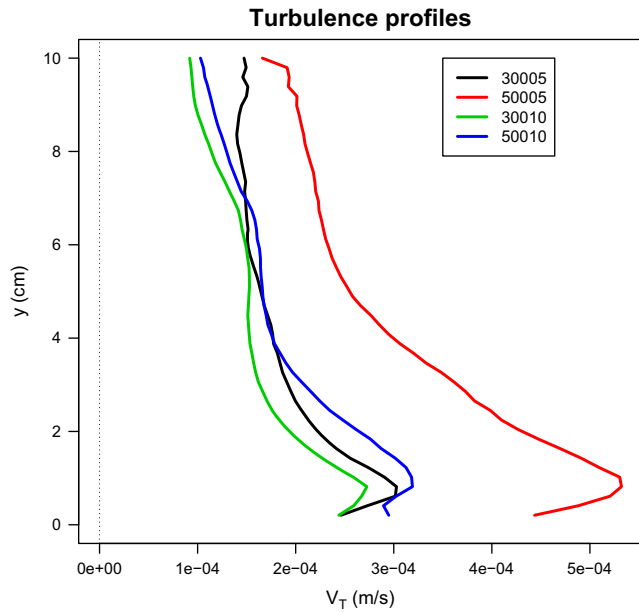


Fig. 12. Vertical profiles of the averaged magnitude of the velocity vector at the front and inside the primary vortex are determined as described in Section 2.

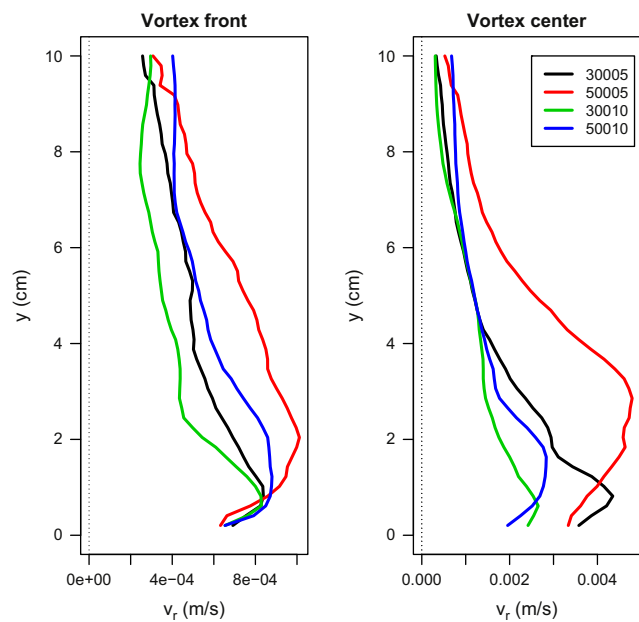


Fig. 13. Vertical profiles of the averaged magnitude of the velocity vector at the front and inside the primary vortex are determined as described in Section 2.

difference (i.e.,  $F$ ). Variations in  $F$  were found to lead to changes in the characteristic time of flow evolution. We found an expression for the characteristic time, derived by dimensionless analysis, that enabled the satisfactory overlapping of experimental curves for all runs. Analysis shows that the microburst exhibits a certain degree of self similarity. Although variations in  $Re$  also appeared to lead to changes in the flow structure, the similarity between our experimental results and those reported by Proctor – i.e., for a  $Re$  value that differed greatly from that used in this study suggests that the

effect on the overall flow structure resulting from variations in  $Re$  is much lesser than that of varying  $F$ .

This study has also shown that vortex structure is highly affected by the type of forcing (jet impingement or density perturbation) used in the simulation. In general, larger density perturbations dampen the fluid velocity upstream of the main vortex. An important consequence is that a well-organized succession of vortices only happens when both high density perturbation and low jet flux are used, because both processes favor smaller velocities of the fluid elements. On the other hand, when a more intense jet is combined with smaller density perturbation, the large velocities inhibit the formation of well-defined secondary vortices after the primary one. These results may be explained as a consequence of increased momentum diffusion when either forcing favors larger velocities of the fluid elements.

The good agreement between our experimental results and previous simulations, such as those by Proctor (1988) and by Vermeire et al. (2011) show that our experimental setup can be used as a starting point for the study of other problems such as the effect of the topology and vegetation on the evolution of microburst.

### Acknowledgments

This research was support by CSIC and PEDECIBA, Uruguay and Conselho Nacional de Desenvolvimento Científico e Tecnológico (CNPQ), Brazil.

### References

Adrian, R., 1991. Particle-imaging techniques for experimental fluid mechanics. *Annual Review of Fluid Mechanics* 23, 261–304.

Anabor, V., Rizza, U., Nascimento, E.L., Degrazia, G.A., 2011. Large-eddy simulation of a microburst. *Atmospheric Chemistry and Physics* 11, 9323–9331.

Fujita, T., 1985. The downburst, microburst and macroburst, satellite and mesometeorology research project (smrp). Department of Geophysical Science 210, 122.

Fujita, T., 1990. Downbursts: meteorological features and wind field characteristics. *Journal of Wind Engineering and Industrial Aerodynamics* 36, 75–86.

Hjelmfelt, M., 1987. The microburst of 22 June 1982 in jaws. *Journal of Atmospheric Sciences* 44 (12), 1646–1665.

Hjelmfelt, M., 1988. Structure and life cycle of microburst outflows observed in Colorado. *Journal of Applied Meteorology* 27, 900–927.

Holmes, J., Oliver, S., 2000. An empirical model of a downburst. *Engineering Structures* 22, 1167–1172.

Kim, J., Hangan, H., 2007. Numerical simulations of impinging jets with application to downbursts. *Journal of Wind Engineering and Industrial Aerodynamics* 95, 279–298.

Landreth, C.C., Adrian, R.J., 1990. Impingement of a low Reynolds number turbulent circular jet onto a flat plate at normal incidence. *Experiments in Fluids* 9, 74–84.

Lundgren, T., Yao, J., Mansour, N., 1992. Microburst modelling and scaling. *Journal of Fluid Mechanics* 239, 461–488.

Mason, M., Letchforda, C., James, D., 2005. Pulsed wall jet simulation of a stationary thunderstorm downburst. Part A. Physical structure and flow field characterization. *Journal of Wind Engineering and Industrial Aerodynamics* 93, 557–580.

Proctor, F.H., 1988. Numerical simulations of an isolated microburst. Part I. Dynamics and structure. *Journal of Atmospheric Sciences* 45, 3137–3160.

Proctor, F.H., 1989. Numerical simulations of an isolated microburst. Part II. Sensitivity experiments. *Journal of Atmospheric Sciences* 46, 2143–2165.

Vermeire, B.C., Orf, L.G., Savory, E., 2011. Improved modelling of downburst outflows for wind engineering applications using a cooling source approach. *Journal of Wind Engineering and Industrial Aerodynamics* 99, 801–814.

Wakimoto, R.M., 2001. Convectively-driven high wind events. *American Meteorological Society* 28, 255–298.

Weisman, M.L., 1993. The genesis of severe, long-lived bow echoes. *Journal of Atmospheric Sciences* 50, 645–670.

Westerweel, J., 1997. Fundamentals of digital particle image velocimetry. *Measurement Science and Technology* 8, 1379–1392.

Westerweel, J., 2000. Theoretical analysis of the measurement precision in particle image velocimetry. *Experiments in Fluids* 29, 3–12.